



Characterization of the magnetic properties of a $\text{GdBa}_2\text{Cu}_3\text{O}_7/\text{La}_{0.75}\text{Sr}_{0.25}\text{MnO}_3$ superlattice using off-axis electron holography

T. Kasama^{a,b}, M.S. Moreno^{b,c}, R.E. Dunin-Borkowski^{b,a,*}, S.B. Newcomb^d,
N. Haberkorn^{c,e}, J. Guimpel^{c,f}, P.A. Midgley^b

^a Frontier Research System, The Institute of Physical and Chemical Research, Hatoyama, Saitama 350-0395, Japan

^b Department of Materials Science and Metallurgy, University of Cambridge, Pembroke Street, Cambridge CB2 3QZ, UK

^c Centro Atómico Bariloche, Comisión Nacional de Energía Atómica, San Carlos de Bariloche, 8400 Rio Negro, Argentina

^d Glebe Scientific Limited, Glebe Laboratories, Newport, Co. Tipperary, Ireland

^e Universidad Nacional del Sur, Avda. Alem 1253, Bahía Blanca, 8000 Bs. As., Argentina

^f Instituto Balseiro, Universidad Nacional de Cuyo, San Carlos de Bariloche, 8400 Rio Negro, Argentina

Available online 28 October 2005

Abstract

Off-axis electron holography is used to characterize the magnetic properties of a $\text{GdBa}_2\text{Cu}_3\text{O}_7/\text{La}_{0.75}\text{Sr}_{0.25}\text{MnO}_3$ superlattice below the Curie temperature of the manganite layers, in both cross-sectional and plan-view geometry. The samples were prepared for electron microscopy using focused ion beam milling. Differences between the magnetic properties of successive manganite layers are observed in the cross-sectional sample. Magnetic ripple contrast and weakly magnetic regions are observed in plan-view geometry. Although the results may be affected by sample preparation for electron microscopy, the observed differences between the magnetic properties of the manganite layers are consistent between the different samples examined.

© 2005 Elsevier B.V. All rights reserved.

PACS: 75.47.Lx; 75.70.Cn; 42.40.Kw

Keywords: Manganite; High- T_C superconductor; Superlattice; Cross-sectional sample geometry; Off-axis electron holography; Focused ion beam milling

1. Introduction

High- T_C cuprate/doped-manganite $\text{RBa}_2\text{Cu}_3\text{O}_7/\text{La}_{1-x}\text{A}_x\text{-MnO}_3$ ($R = \text{Y, Gd}$; $A = \text{Ca, Sr, Ba}$) layered structures, which are usually strained as a result of small differences in lattice parameter between the constituent materials, exhibit interesting magnetic and superconducting properties that are sensitive to local variations in interatomic spacing and bond angle in the layers. They are of interest for use in spintronic devices, whose properties will depend on their layer structure, defect topology and interface quality.

Recently, the presence of an unexpected antiferromagnetic (AF) phase has been inferred in $\text{YBa}_2\text{Cu}_3\text{O}_7/\text{La}_{0.67}\text{Ca}_{0.33}\text{MnO}_3$ superlattices from hysteresis loops that show exchange coupling at 5 K [1]. The microscopic origin of this AF phase

was not established. Here, we report on a preliminary study of the magnetic properties of a similar $\text{GdBa}_2\text{Cu}_3\text{O}_7/\text{La}_{0.75}\text{Sr}_{0.25}\text{MnO}_3$ (GBCO/LSMO) superlattice, both below and above the Curie temperature of the manganite layers, using off-axis electron holography in the transmission electron microscope (TEM).

Off-axis electron holography can be used to measure the magnetic induction in a thin-film structure with a spatial resolution that can approach the nanometer scale [2]. The technique involves the measurement of the phase shift of a high-energy electron wave that has passed through a material. The phase shift is sensitive to the local electrostatic potential (the mean inner potential) of the sample and to its magnetic induction. In the absence of dynamical diffraction, the phase shift is given by the expression

$$\phi(x) = C_E \int V_0(x, z) dz - \left(\frac{e}{\hbar}\right) \int \int B_{\perp}(x, z) dx dz \quad (1)$$

* Corresponding author. Tel.: +44 1223 334564; fax: +44 1223 334563.

E-mail address: rafal.db@msm.cam.ac.uk (R.E. Dunin-Borkowski).

where z is the incident electron beam direction, x a direction in the plane of the sample, V_0 the mean inner potential, B_{\perp} the component of magnetic induction perpendicular to both x and z , and C_E is an energy-dependant constant that takes a value of $6.53 \times 10^6 \text{ rad V}^{-1} \text{ m}^{-1}$ at a microscope accelerating voltage of 300 kV.

Although the magnetic properties of manganite films have been studied using electron holography in the past, the complexity of their magnetic phase diagrams, together with their sensitivity to small variations in composition and strain, suggests that further work is required to understand the magnetic properties of such materials fully [3–7]. In particular, none of these studies were performed on layered manganite structures in cross-section, both because such measurements involve the measurement of weak magnetic signals and because they are complicated by contributions to the measured signal from diffraction and Fresnel contrast (see below) [8,9].

2. Experimental details

GBCO/LSMO superlattices were grown epitaxially onto SrTiO_3 (0 0 1) substrates by dc magnetron sputtering [10]. The sample studied here consists of a superlattice of five GBCO and four LSMO layers, with average layer thicknesses of 19.0 and 9.2 nm, respectively, as shown in the form of a schematic diagram in Fig. 1. The labeling of the LSMO layers (top, second, third, bottom), which are referred to in the text below, is defined in this diagram.

Samples were prepared for electron microscopy by using focused ion beam (FIB) milling with Ga ions at 30 kV in an FEI 200 FIB workstation. A Pt strap was deposited onto the sample surface in order to minimize any ion damage during subsequent FIB milling. Cross-sectional samples were prepared in standard ‘trench’ geometry, while plan-view samples were made by milling away the SrTiO_3 substrate from beneath the layers. Great care was taken to minimize damage to the sample by milling with a low beam current parallel to the surface of the final membrane. Although FIB milling is known to damage the surfaces of thin

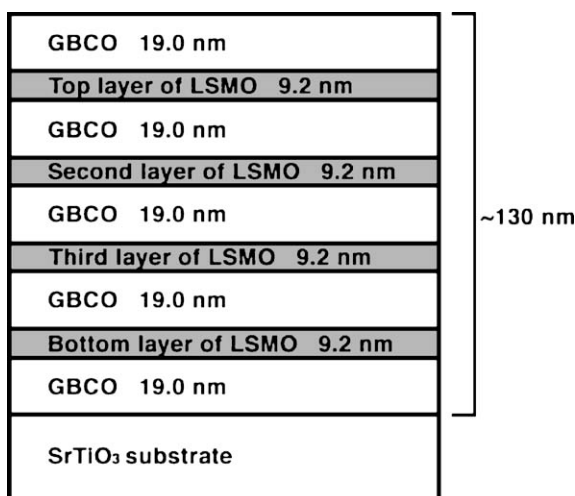


Fig. 1. Schematic diagram of the GBCO/LSMO superlattice examined in this study. The average thicknesses of the layers were determined by HRTEM.

TEM specimens, it provides the great advantage for electron holography of eliminating the rapid specimen thickness variations that often result from Ar ion milling layered structures.

A Philips CM300-ST field emission gun (FEG) TEM was used to acquire high-resolution (HR) lattice images and off-axis electron holograms of the samples at 300 kV. A bright-field image and an electron hologram of a cross-sectional sample of the layered structure are shown in Fig. 2a and b, respectively. Fig. 2c shows a schematic ray diagram illustrating the electron microscope geometry for electron holography. The sample is illuminated coherently, with the region of interest positioned so that it covers approximately half the field of view. An electron biprism is used to overlap the electron wave that has passed through the sample with a reference wave that has passed only through vacuum. Interference of the two parts of the electron wave results in the formation of holographic fringes, which record both the amplitude and the phase shift of the electron wave that has passed through the sample. The use of a ‘Lorentz’ minilens allows holograms of magnetic materials to be acquired at high magnification with the conventional microscope objective lens switched off and the sample in magnetic-field-free conditions. For the present experiments, a biprism voltage of 250 V was used, corresponding to a holographic interference fringe spacing with the sample in field-free conditions of 2.6 nm. Reference holograms were acquired from vacuum alone and used to remove distortions associated with the imaging and recording system of the microscope. Samples were examined at both 90 and 293 K, using a liquid-nitrogen-cooled TEM specimen holder. The LSMO layers were expected to become ferromagnetic below ~ 230 K, while at room temperature no magnetic signal was expected from the sample. Holograms were always acquired at remanence after saturating the sample magnetically parallel to the layers in the cross-sectional sample, or to the sample edge in the plan-view sample, by using the field of the conventional microscope objective lens to apply in-plane fields of ~ 1 T with the sample tilted at $\pm 30^\circ$. Each sample was tilted back to 0° in zero field for electron holography. Pairs of phase images that had been acquired with the sample magnetized in opposite directions were used to eliminate the unwanted mean inner potential contribution to the phase shift (see below). Further details of the procedure used to record electron holograms and to extract phase information from them are described elsewhere [2].

3. Results and discussion

3.1. HRTEM observations

An HRTEM image of the uppermost LSMO and GBCO layers in the cross-sectional sample is shown in Fig. 3. Lattice fringes were observed in all of the layers of interest, although approximately half of the top GBCO layer was amorphized, presumably as a result of the unintentional ion damage that occurred during the deposition of the protective Pt strap. In addition, the spacing of the lattice fringes visible within the uppermost GBCO layer is slightly different from that in the other layers in this sample. In Fig. 3, the interfaces between the

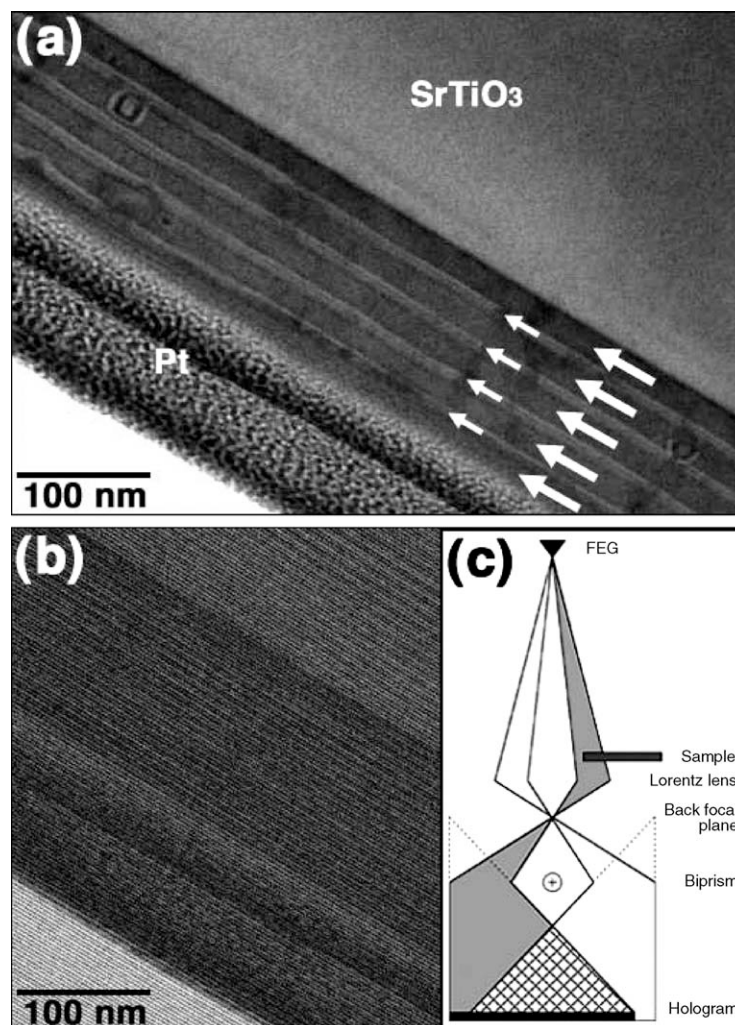


Fig. 2. (a) Bright-field TEM image of the GBCO/LSMO superlattice, imaged in cross-sectional geometry. The large and small arrows indicate the GBCO and LSMO layers, respectively. The Pt originates from TEM sample preparation using FIB milling. (b) Representative off-axis electron hologram of the area shown in (a). (c) Schematic illustration of the setup used to generate off-axis electron holograms. Essential components are the field emission gun (FEG) electron source, which is used to provide coherent illumination, and the electron biprism, which is used to overlap the sample and reference waves. The Lorentz minilens allows the sample to be imaged with an optimal field of view in magnetic-field-free conditions.

LSMO and GBCO layers are indistinct, and the layers are not always uniform in thickness. In a separate study, similar samples containing individual GBCO layers were characterized to have interface roughnesses of ~ 1.1 nm, with $\sim 30\%$ interdiffusion of LSMO into the first unit cell (~ 1.1 nm) of the GBCO layer [11]. In the present sample, the average thicknesses of the LSMO and GBCO layers were measured by HRTEM to be 9.2 and 19.0 nm, respectively.

3.2. Predicted phase shift in cross-sectional geometry

If neither V_0 nor B_{\perp} vary with z within a sample of thickness t , and if there are no (demagnetizing) fields outside the sample, then Eq. (1) can be simplified to

$$\phi(x) = C_E V_0(x)t(x) - \left(\frac{e}{\hbar}\right) \int B_{\perp}(x)t(x) dx \quad (2)$$

In a sample of uniform thickness and composition, the in-plane magnetic induction is therefore expected to be proportional to

the gradient of the measured phase shift. On the assumption that the sample thickness is uniform, that only the LSMO layers are magnetic and that they are magnetized perpendicular to the electron beam direction, the phase shift in the present cross-sectional sample that would be predicted using Eq. (2) is shown in Fig. 4. The parameters used in the calculation are given in the caption to the figure. If the magnetic induction is the same in magnitude and direction in each LSMO layer, then the magnetic contribution to the phase shift is predicted to have the appearance of a staircase, rising in each LSMO layer and remaining flat in each GBCO layer, as shown in Fig. 4a. The phase gradient in each LSMO layer is then proportional to the magnitude of the induction. The mean inner potential contribution to the phase shift is shown in Fig. 4b, on the assumption (based on experimental measurements presented below) that V_0 for LSMO is slightly larger than that for GBCO. The total phase shift, which would be measured experimentally from a single electron hologram, is shown in Fig. 4c. As a result of the fact that the mean inner potential contribution is much

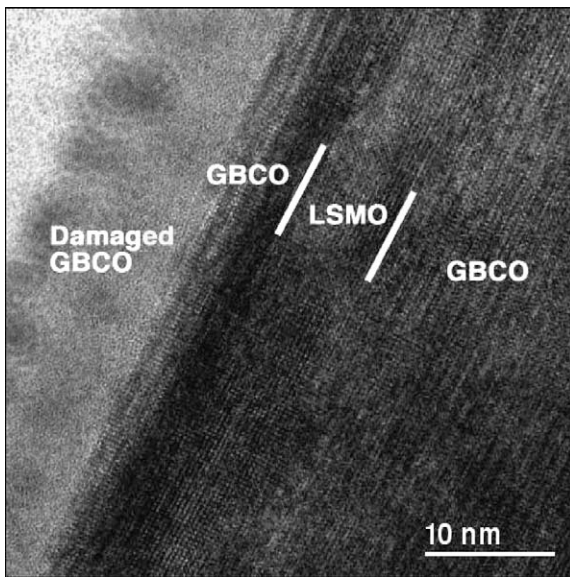


Fig. 3. HRTEM image of the uppermost GBCO/LSMO layers in a cross-sectional sample prepared using FIB milling. The GBCO layers exhibit contrast that has a periodicity of ~ 1.17 nm. The top GBCO layer is partly damaged and amorphized as a result of Pt deposition during FIB sample preparation.

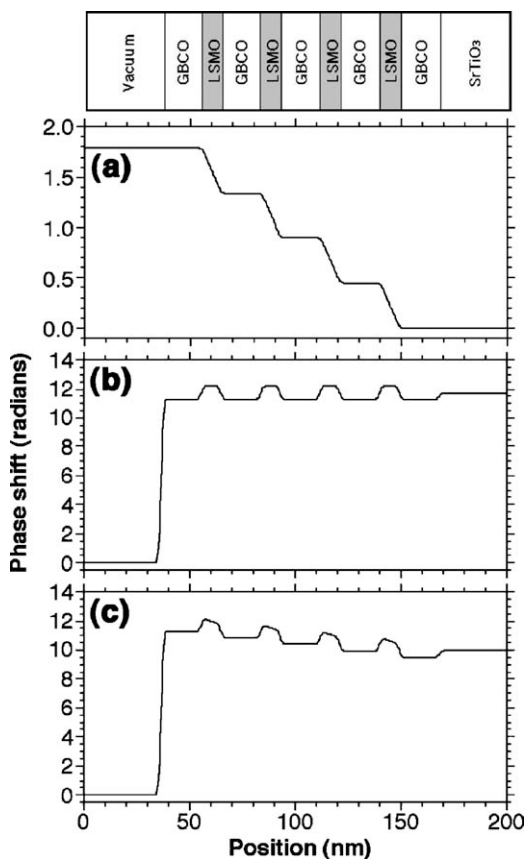


Fig. 4. Phase profiles showing (a) the magnetic contribution, (b) the mean inner potential contribution and (c) the total phase shift, predicted for a cross-sectional sample that has a uniform thickness of 100 nm containing the GBCO/LSMO superlattice. The following values were used as input parameters: magnetic induction of LSMO = 0.32 T [12]; mean inner potentials of LSMO, GBCO and SrTiO₃ = 18.7, 17.3 and 18.0 V; layer thicknesses of LSMO and GBCO = 9.2 and 19.0 nm.

larger than the magnetic contribution, the magnetic signal of primary interest must be separated carefully from the mean inner potential contribution to the total phase shift. This separation was achieved by taking either half of the sum or half of the difference between phase images that had been recorded with the sample magnetized in opposite directions. These images provided the mean inner potential and magnetic contributions to the phase shift, respectively, on the assumption that the magnetic microstructure in the sample has reversed exactly between the two recorded phase images. The sample is also assumed to remain magnetized in the plane of the specimen at remanence. Both of these assumptions are expected to hold for the cross-sectional and plan-view sample geometries examined here.

3.3. Magnetic observations in cross-sectional geometry

Fig. 5 shows experimental measurements of the mean inner potential and magnetic contributions to the phase shift, obtained from the cross-sectional sample using the approach described above. The positions of the LSMO layers are shown in gray in Fig. 5b–d. The measured mean inner potential profile

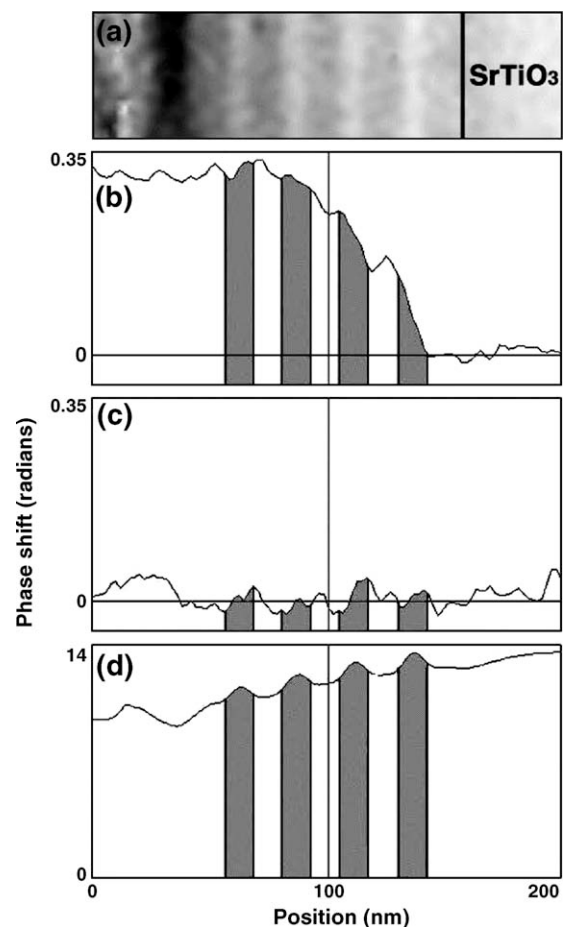


Fig. 5. (a) Experimental measurement of the mean inner potential contribution to the phase shift, and profiles showing (b and c) the magnetic contributions and (d) the mean inner potential contribution to the phase shift at (b) 90 K and (c and d) 293 K. The positions of the LSMO layers are shown in gray in (b)–(d).

(Fig. 5d) is reassuringly similar to the predicted profile shown in Fig. 4b. The gentle slope in the experimental profile is thought to result from a gradual decrease in sample thickness towards the specimen edge (Fig. 5d). The measured magnetic contribution to the phase shift is observed to decrease in the manner of a staircase at 90 K (Fig. 5b), with significant changes in phase always occurring at the positions of the LSMO layers. This behavior is also qualitatively consistent with the simulated profile shown in Fig. 4a. Additional features in the experimental profile may result from a slightly different defocus having been used to record the two individual phase images with the sample magnetized in opposite directions. The resulting Fresnel fringes at the positions of the interfaces may then not have cancelled exactly. The magnetic contribution to the phase shift is close to zero at 293 K (Fig. 5c), which is consistent with the expected absence of a magnetic signal above the Curie temperature of the manganite layers (~ 210 K) [1].

From a comparison of Figs. 4 and 5, it is interesting to note that experimentally the magnetic signal from the LSMO layers is smaller than in the simulated profiles, whereas the mean inner potential profiles are similar in magnitude. By examining the measured mean inner potential contribution to the phase shift (Fig. 5d), the specimen thicknesses of the LSMO layers are inferred to be 93, 100, 106 and 111 nm, by using the first term in Eq. (2) and assuming a value for V_0 of 18.7 V. However, these values include regions close to the sample surfaces that may be magnetically dead as a result of FIB milling. It is not easy to measure the thicknesses of magnetically dead layers on sample surfaces experimentally, particularly if the magnetization of the sample is unknown. However, based on a related study of patterned spin-valve structures [13], they are expected to have thicknesses of at least 20 nm on each sample surface. Table 1 shows that, on the assumption that the magnetically dead layer thickness is either 20, 25 or 30 nm on each sample surface, the experimentally measured magnetic induction is always inferred to be smaller than the value of 0.32 T expected from bulk measurements [12]. These values are discussed further below. The slightly negative value of induction inferred for the top layer is likely to result from noise in the experimental profile.

Table 1

Specimen thicknesses calculated at the positions of the LSMO layers from the mean inner potential contribution to the phase shift measured from the FIB-prepared cross-sectional sample, and magnetic inductions in these layers inferred on the assumption of various magnetically dead layer thicknesses

Layer	Specimen thickness (nm) ^a	Magnetic phase shift (rad)	Magnetic induction (T)		
			20 nm ^b	25 nm ^b	30 nm ^b
Top	93	-0.021	-0.03	-0.04	-0.05
Second	100	0.064	0.08	0.09	0.11
Third	106	0.086	0.09	0.11	0.13
Bottom	111	0.158	0.16	0.19	0.22

^a Calculated from the measured mean inner potential contribution to the phase shift shown in Fig. 5d, using a value of V_0 for LSMO of 18.7 V.

^b This is the magnetically dead layer thickness assumed to be present on each sample surface.

The most striking aspect of Fig. 5 is that each LSMO layer appears to be less magnetic than the previous one, with increasing distance from the substrate. Consistent phase profiles demonstrating this trend were obtained from several different regions of the sample, of different specimen thickness. Although the uppermost LSMO layer may have been ion damaged during the early stages of the FIB sample preparation (Fig. 3), HRTEM observations revealed lattice fringes in all of

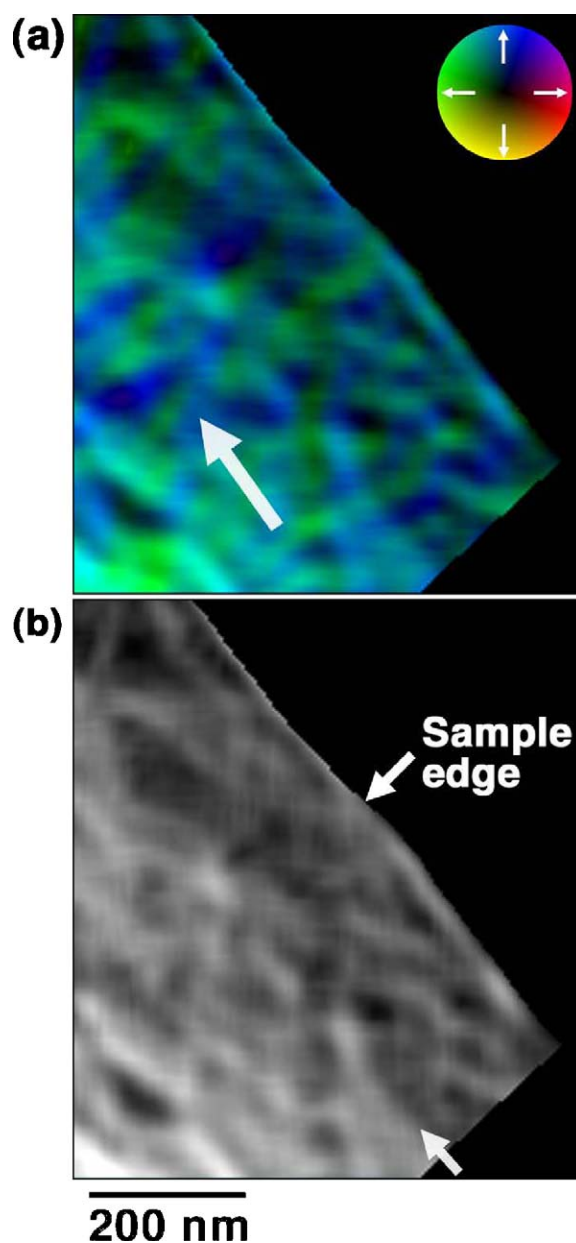


Fig. 6. (a) Direction and (b) magnitude of the magnetic induction measured using electron holography at remanence from the FIB-prepared plan-view sample. The average direction of the magnetic induction is shown using a large arrow in (a). The local induction is indicated according to a color wheel. The sample was saturated magnetically parallel to its edge before removing the applied field and recording the hologram. The small arrow in (b) indicates the boundary between single-layer and two-layer regions in the sample. The mean inner potential contribution has been subtracted from the measured phase image (see text for details). (For interpretation of the references to color in this figure legend, the reader is referred to the web version of the article.)

the LSMO layers that were studied using electron holography. The observed change in magnetic properties with layer number may therefore be a real property of the sample, rather than resulting from TEM sample preparation.

3.4. Magnetic observations in plan-view geometry

An FIB-prepared plan-view sample containing the same layer structure was examined at 90 K. Fig. 6 shows the measured magnetic induction at remanence, after saturating the sample magnetically parallel to its edge. In Fig. 6, the mean inner potential contribution, which was obtained by averaging phase images acquired with the sample magnetized in several different directions, has been subtracted from the measured phase shift. The average direction of induction in the sample, which is shown according to a color wheel, is seen to follow the direction of the applied magnetic field, as indicated by the arrow in Fig. 6a. In addition, even though the sample is a single crystal, magnetic ripple contrast is visible, with the induction in adjacent regions rotating by angles of $\sim 90^\circ$. The predominant texture of the ripple contrast is perpendicular to the average magnetization direction of the film, as a result of local perturbations of its easy axis [14]. No magnetic signal was apparent at 293 K, as expected from the Curie temperature of the manganite layers and from the observations from the cross-sectional sample.

Interestingly, two regions with different magnetic contrast, with a sharp boundary between them, are visible in Fig. 6a. This effect is likely to result from the presence of different numbers of LSMO layers in projection in different regions of the thin film after preparation for electron microscopy. Up to a distance of ~ 210 nm from the specimen edge, only one LSMO layer is present. Two layers then contribute to the contrast, with the two-layer region exhibiting approximately twice the phase gradient and having twice the measured sample thickness of the single-layer region.

The magnetic induction measured from the plan-view sample is 0.23 T in the single-layer region and 0.20 T on average in each layer in the two-layer region, on the assumption that the LSMO layers are magnetic through their entire thickness. This observation is consistent with a magnetically dead layer thickness of 30 nm on each surface of the cross-sectional sample, if the magnetic signal in the plan-view sample originates from the two LSMO layers that are closest to the SrTiO₃ substrate. However, the saturation magnetization expected from bulk measurements is 0.32 T at 90 K [12]. This difference may be explained by the formation of magnetization ripple in the cross-sectional sample, as observed in the plan-view sample in Fig. 6a. It may also be associated with the presence of weakly magnetic regions in the film at remanence, which can be seen by plotting the magnitude of the magnetic induction measured in the plan-view sample in Fig. 6b, or alternatively with a magnetic thickness for the LSMO layers that is smaller than their physical thickness.

The weakly magnetic regions that are visible in Fig. 6b are distributed randomly. Their presence in the single-layer region

suggests that they do not arise from the superposition of oppositely magnetized regions in two layers that are viewed in projection. They may be associated with the AF phase reported by Haberkorn et al. [1], although the possibility of local damage during sample preparation cannot be excluded completely. On the assumption (mentioned above) that the two LSMO layers that are closest to the SrTiO₃ substrate contribute to the magnetic signals observed in Fig. 6, and that the magnetically dead layer thickness is 30 nm on each sample surface, the ratio of the magnetic signals in these two layers is measured to be 0.59 in the cross-sectional sample and 0.70 in the plan-view sample. The consistency between these values is encouraging, and supports the fact that the observed decrease in magnetization in the upper LSMO layers may be a real property of the layers, perhaps related to the density of the weakly magnetic regions observed in the plan-view sample, rather than resulting from the effects of TEM sample preparation.

4. Conclusion

Quantitative information about magnetic remanent states in a GBCO/LSMO superlattice has been obtained in both cross-sectional and plan-view geometry using off-axis electron holography. Measurements obtained from samples that were prepared using FIB milling show clear magnetic signals at 90 K from the LSMO layers, whereas no magnetic signals were observed at 293 K. The magnetic induction in the LSMO layers is observed to decrease with increasing layer number from the substrate. Although this decrease may result from TEM sample preparation, we suggest that it may originate from an increase in the density of weakly magnetic regions in the uppermost LSMO layers. Magnetic ripple contrast is also observed in the single-crystalline LSMO layers in plan-view geometry.

Acknowledgements

We thank the Royal Society, UK and CONICET, Argentina for supporting this work.

References

- [1] N. Haberkorn, J. Guimpel, M. Sirena, L.B. Steren, W. Saldarriaga, E. Baca, M.E. Gómez, *Appl. Phys. Lett.* 84 (2004) 3927.
- [2] R.E. Dunin-Borkowski, M.R. McCartney, D.J. Smith, in: H.S. Nalwa (Ed.), *Encyclopedia of Nanoscience and Nanotechnology*, vol. 3, American Scientific Publishers, California, USA, 2004, pp. 41–100.
- [3] J.C. Loudon, N.D. Mathur, P.A. Midgley, *Nature* 420 (2002) 797.
- [4] J.H. Yoo, Y. Murakami, D. Shindo, T. Atou, M. Kikuchi, *Phys. Rev. B* 66 (2002) 212406.
- [5] Y. Murakami, J.H. Yoo, D. Shindo, T. Atou, M. Kikuchi, *Nature* 423 (2003) 965.
- [6] J.H. Yoo, Y. Murakami, D. Shindo, T. Ohsuna, *Philos. Mag.* 84 (2004) 2597.
- [7] J.H. Yoo, Y. Murakami, D. Shindo, T. Atou, M. Kikuchi, *Phys. Rev. Lett.* 93 (2004) 047204.
- [8] R.E. Dunin-Borkowski, M.R. McCartney, D.J. Smith, S.S.R. Parkin, *Ultramicroscopy* 74 (1998) 61.
- [9] T. Tanji, S. Hasebe, Y. Nakagami, K. Yamamoto, M. Ichihashi, *Microsc. Microanal.* 10 (2004) 146.

- [10] J. Guimpel, B. Maiorov, E. Osquiguil, G. Nieva, F. Pardo, *Phys. Rev. B* 56 (1997) 3552.
- [11] N. Haberkorn, J. Guimpel, L.B. Steren, G. Campillo, W. Saldarriaga, M.E. Gómez, *J. Appl. Phys.* 94 (2003) 3011.
- [12] N. Haberkorn, Unpublished data, 2005.
- [13] T. Kasama, P. Barpanda, R.E. Dunin-Borkowski, S.B. Newcomb, M.R. McCartney, F.J. Castaño, C.A. Ross, *J. Appl. Phys.* 98 (2005) 013903.
- [14] H. Kronmüller, M. Fähnle, *Micromagnetism and the Microstructure of Ferromagnetic Solids*, Cambridge University Press, Cambridge, UK, 2003, 432 pp.